BOLETIN DE LA SOCIEDAD ESPAÑOLA DE
Cerámica y Vidrio
www.elsevier.es/bsecv

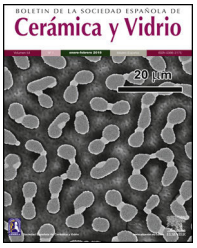

Original

Effect of annealing and potassium substitution on the thermoelectric and magnetic properties of directionally grown $Bi_2Sr_2Co_2O_y$ ceramics

Gizem Çetin[a,*], *Bekir Özçelik*[a], *Mehmet Gürsul*[a], *Miguel Angel Torres*[b], *Maria A. Madre*[b], *Andres Sotelo*[b]

[a] *Department of Physics, Faculty of Sciences and Letters, Çukurova University, 01330 Adana, Turkey*
[b] *ICMA (CSIC-Universidad de Zaragoza), C/María de Luna 3, 50018 Zaragoza, Spain*

ARTICLE INFO

Article history:
Received 23 May 2019
Accepted 5 August 2019
Available online 21 August 2019

Keywords:
Thermoelectric oxides
Texture
Microstructure
Electrical properties
Magnetic properties

ABSTRACT

$Bi_2Sr_{2-x}K_xCo_2O_y$ ($x = 0.0$, 0.025, 0.050, 0.075, 0.100, 0.125, and 0.15) ceramic materials have been fabricated using a classical ceramic process, followed by texturing through directional solidification. SEM analysis of samples, before and after annealing has shown that grains were aligned along the growth direction. While as-grown samples have several phases, besides the thermoelectric one, the annealed ones show much higher thermoelectric phase content. In addition, K-substitution increases the thermoelectric phase content and enhances grain orientation. These improvements decrease the electrical resistivity without significant changes in Seebeck coefficient. The maximum power factor value for 0.10K-substituted annealed samples has been found as 0.20 $mW/K^2 m$. This is superior to the highest reported for hot-pressed materials. However, all samples have similar magnetic properties.

Efecto del recocido y el dopado con potasio en las propiedades termoeléctricas y magnéticas de las cerámicas $Bi_2Sr_2Co_2O_y$ crecidas direccionalmente

Palabras clave:
Óxidos termoeléctricos
Textura
Microestructura
Propiedades eléctricas
Propiedades magnéticas

RESUMEN

Materiales cerámicos de composición $Bi_2Sr_{2-x}K_xCo_2O_y$ ($x = 0.0$, 0.025, 0.050, 0.075, 0.100, 0.125, y 0.15) se han preparado por medio del proceso cerámico tradicional, seguido por un texturizado a través de una solidificación direccional. El análisis de las muestras por medio del SEM, antes y después del recocido, ha mostrado que los granos se han alineado en la dirección del crecimiento. Mientras que las muestras crecidas presentan varias fases, además de la termoeléctrica, las recocidas tienen mayor cantidad de fase termoeléctrica. Además, la substitución con potasio aumenta la proporción de fase termoeléctrica y mejora

* *Corresponding author.*
E-mail address: gcetin@cu.edu.tr (G. Çetin).
https://doi.org/10.1016/j.bsecv.2019.08.004

la orientación de los granos. Estas mejoras llevan a una disminución de la resistividad eléctrica sin modificar en gran medida el coeficiente de Seebeck. El mayor valor del factor de potencia se ha obtenido en muestras recocidas con substituciones del 0.10 K, 0.20 mW/K^2 m. Este valor es mayor que el mayor reportado en materiales texturizados por prensado uniaxial en caliente. Sin embargo, la diferencia en el contenido de K, no produce variaciones en las propiedades magnéticas.

Introduction

At present, researchers are looking for solutions to global energy crises and saving the environment from the outcomes of wasted heat. For this purpose, thermoelectric (TE) materials are ideal to utilize, as they can harvest wasted heat, transforming it into useful electrical energy [1–3]. Furthermore, thermoelectric materials can also work in air conditioning systems [2–4] or electric power generation [2,5]. Quantification of performances is performed through the figure-of-merit, ZT ($=TS^2/\rho\kappa$; T is temperature, S the Seebeck coefficient, ρ electrical resistivity, and κ is the thermal conductivity) [6].

Commercially available TE devices are produced from metallic materials or compounds, e.g. Bi_2Te_3 and PbTe, with large ZT (∼1) at low-medium temperature [7–9]. Therefore, these systems cannot use to harvest the high-temperature wasted heat. In addition, these compounds usually content heavy or toxic elements which can be degraded or released at high temperatures.

The feasibility for obtaining materials which can work at elevated temperature started in 1997, with the fabrication of $NaCo_2O_4$ ceramics with attractive thermoelectric properties [10]. This finding allowed a large amount of study on similar ceramic systems, as $Ca_3Co_4O_9$ (349), $La_{1-x}AE_xCoO_3$, or $Bi_2AE_2Co_2O_x$ (AE = alkaline earth) [11–16], which showed hole conduction. Moreover, extended studies on other oxides allowed discovering materials, such as MnO- or TiO-based ones [17,18], with electron conduction. Consequently, both types can be combined to build practical TE devices.

Crystallographically, these CoO-based thermoelectric materials can be described as a monoclinic structure composed of two subsystems, a common conducting one with CdI_2 crystal structure with CoO_2 composition, and a separating one with NaCl structure (RS), where the other cations can be accommodated. Both substructures only differ in the b lattice parameter, which produces a misfit in this axis [19,20]. Moreover, the anisotropic crystal structure in these materials leads to large anisotropic electrical properties, as for example, S can be tuned up through modifications of misfit factor or the oxidation state of cations in the RS substructure [21]. These modifications can be performed through different procedures, as cation substitutions [22–28], or texturing techniques [29–31].

It has been argued that the materials having a superlattice structure, in which conducting and insulating layers are successively stacked, can facilitate high thermoelectric performance [32]. According to these arguments, the Seebeck coefficient in the direction of piling would enhance due to the increasing of density of state of carriers produced by the two-dimensionality. In addition, decrease in thermal conductivity would be expected depending on to phonon scattering at the interface between layers [33]. On the other hand, the $Bi_2Sr_2CaCu_2O_x$ (Bi-2212) is known an oxide superconductor with a superlattice structure in which conducting (Cu–O) and insulating (Bi–O) layers alternate. Since Bi-2212 materials have low thermoelectric properties, Co is substituted for Cu in the Bi-2212 phase to form $Bi_2Sr_2Co_2O_x$ polycrystalline materials [33]. According to our knowledge Na and K doping in Bi-2212 provides high Tc values and improves the physical properties when the samples are prepared via partial or total melting [34,35]. Taking into account the same analogy, we have previously studied Na and K substitution for Sr [27,28].

In those studies, we have prepared our samples via solid state route. But, the objective of this work is studying the modifications induced by partial Sr by K replacement in the structural, microstructural, and TE properties of $Bi_2Sr_2Co_2O_y$ materials prepared by laser floating zone (LFZ).

Experimental

Polycrystalline $Bi_2Sr_{2-x}K_xCo_2O_y$ ($x = 0$, 0.025, 0.05, 0.075, 0.10, 0.125, and 0.15) ceramics were fabricated using a ceramic route, from Bi_2O_3 (99%, Panreac), $SrCO_3$ (99%, Panreac), K_2CO_3 (99%, Panreac), and CoO (99.99%, Aldrich). Stoichiometric amounts of each compound were mixed and ball milled 30 min at 300 rpm with distilled water, which was evaporated from the slurries using infrared lamps. After drying, the resulting powders were manually milled and subjected to two step calcination procedure for 12 h at 750 and 800 °C, to eliminate CO_2 from the metallic carbonates. These steps will avoid the CO_2 presence in the melting process, which would cause instabilities in the solidification interface [36]. Calcined powders were then pressed in an isostatic press at ∼200 MPa to produce cylindrical bars ($\phi = 2$–3, and length ∼100 mm). These bars were directionally grown from the melt under Nd:YAG laser radiation ($\lambda = 1064$ nm) in a laser floating zone (LFZ) system [37]. The texturing conditions were fixed for all samples, 30 mm/h growth rate. Moreover, the seed was rotated at 3 rpm to produce cylindrical bars, while the seed was rotated in the opposite direction at 15 rpm to maintain the molten zone compositional homogeneity. In these conditions, the textured bars possess constant diameter (ϕ ∼2 mm), but show the presence of several secondary phases formed by their characteristic

incongruent melting [38]. Consequently, the textured materials have been subjected to an annealing process during 24 h at 810 °C, followed by a slow cooling rate to room temperature to produce the TE phase from the secondary ones.

The identification of phases has been made on powdered samples by X-ray diffraction (XRD) from 5° to 60° in a Rigaku D/max-B X-ray powder diffractometer using Cu Kα wavelength. The modification of microstructure, as a function of K doping, was determined by analysing representative images performed on longitudinal polished sections of samples before and after annealing procedure. For this purpose, a field emission scanning electron microscope (FESEM, Zeiss Merlin) has been utilized. Moreover, EDS analysis has been used to determine the phases composition. Furthermore, Archimedes' method has been performed to calculate samples density, using 6.8 g/cm^3 as the theoretical one [39].

ρ and S have been simultaneously measured from 50 to 650 °C in a LSR-3 device (Linseis GmbH). Power factor, PF (=S^2/ρ) was calculated to establish the electrical performances of these samples. Magnetic characteristics were determined using a physical property measurement system (Dyne-cool PPMS, Quantum Design). Magnetic susceptibility has been measured, in zero field cooled (ZFC) mode, under a constant 20 Oe dc applied field and temperatures between 5 and 300 K. On the other hand, in order to determine the magnetic hysteresis cycles, external applied fields from −5 to 5 T, at different temperatures have been used.

Results and discussion

Fig. 1a and b presents the XRD patterns determined on powdered samples before and after annealing, respectively. The diffraction planes displayed in these plots identify the peaks of the TE phase [40]. Furthermore, samples before annealing show the presence of different phases, which have been indexed with the peaks shown with * ($Bi_{0.75}Sr_{0.25}O_y$ [41]), o (Sr-rich Bi-Sr-Co-O [42]), and # (CoO [43]). On the other hand, the patterns presented in Fig. 1a clearly indicate that K-substitution promotes a relative decrease of secondary phases content, when compared with the K-free ones. The comparison of these patterns with their annealed counterparts shown in Fig. 1b, points out to a drastic decrease of secondary phases content through annealing. These patterns also show that the highest peaks are those associated to the *ab*-planes of TE phase. This is a consequence of the large crystal anisotropy, which leads to the formation of very thin platelet grains [44]. The grains shape induces a preferential grain orientation during the samples preparation, and the *c*-axis is mostly perpendicular to the sample holders.

The Lotgering factor (LF) defined as $LF = (P - P_0)/(1 - P_0)$ can be calculated from the intensities of XRD peaks (see Table 1), where P indicates the fraction of the summation of the peak intensities corresponding to the preferred orientation axis to that of the summation of all diffraction peaks in particle-oriented materials and P_0 is *P* of a material with a non-oriented distribution. The LF changes between zero to unity; LF = 0 corresponds to random orientation, and LF = 1 to perfect orientation [45]. As can be seen from Table 1, the LF values of

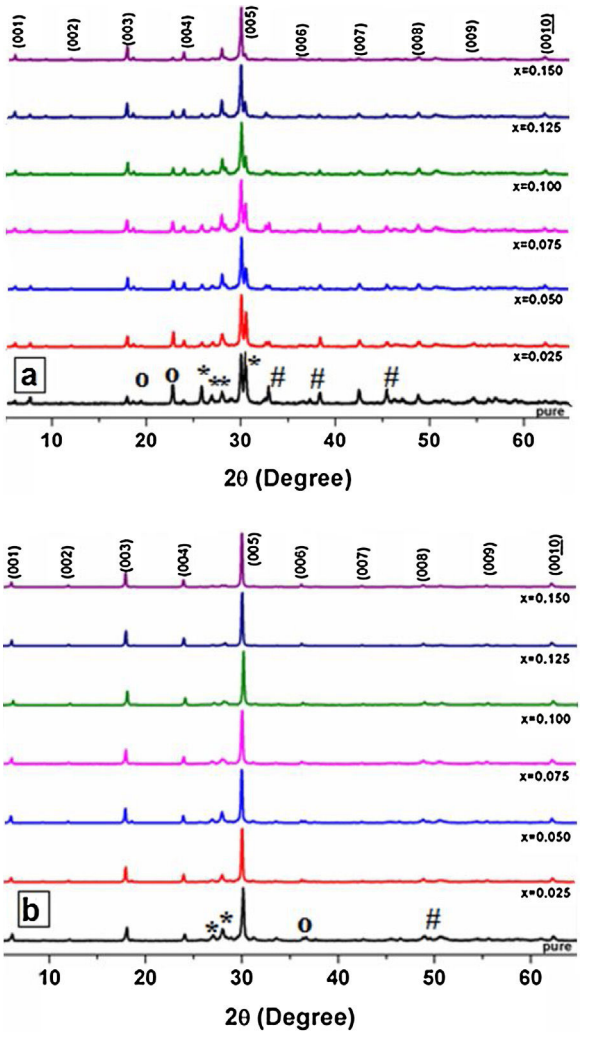

Fig. 1 – Powder XRD patterns of (A) as-grown; and (B) annealed $Bi_2Sr_{2-x}K_xCo_2O_y$ textured samples. The peaks of thermoelectric phase are shown by the diffraction planes. *, o, and # correspond to $Bi_{0.75}Sr_{0.25}O_y$, $CoCo_2O_4$, and $Bi_{3.8}Sr_{11.4}Co_8O_{28.875}$ secondary phases, respectively. Here, a, b, c, d, e, f, and g correspond to $x = 0.0$, 0.025, 0.050, 0.075, 0.10, 0.125, and 0.15, respectively.

annealed samples increase with increasing K-content, pointing out good orientation of the grains.

Fig. 2 presents FESEM micrographs performed on 0.10K-doped samples before and after annealing. As it can be observed, as-grown samples (Fig. 2a) possess good grain orientation along the growth direction and several secondary phases, indicated by arrows for clarity. Black contrast (#1) corresponds to cobalt oxide, dark grey (#2) to Bi-free phase, light grey (#3) to Co-poor phase, and grey (#4) to the thermoelectric $Bi_2Sr_2Co_2O_y$ phase. Other interesting feature not shown here is that K-doping leads to improved grain orientation with the longitudinal rod axis. The grain misalignment, estimated through angle measurement in several SEM micrographs, is ranging from around 13° for undoped samples, to about 7° for the highest K-doped ones. This effect has already been found in other families [46] and has been

Table 1 – Lotgering factors; magnetic parameters; Curie–Weiss temperature, Curie constant, and effective magnetic moment from the Curie–Weiss law.

Sample	Lotgering factor-as-grown	Lotgering factor-annealed fibre	Curie–Weiss temp. θ (K)	Curie constant, C (emu K/g) $\times 10^{-4}$	Effective moment, μ_{eff} (μ_B)
0K	0.59	0.74	−52.46	7.9	2.1
0.025K	0.75	0.82	−45.68	11.4	2.2
0.050K	0.81	0.83	−56.64	10.9	2.3
0.075K	0.77	0.85	−39.04	9.9	2.2
0.100K	0.80	0.89	−48.12	11.2	2.4
0.125K	0.81	0.91	−47.77	10.6	2.3
0.150K	0.87	0.93	−44.21	11.8	2.4

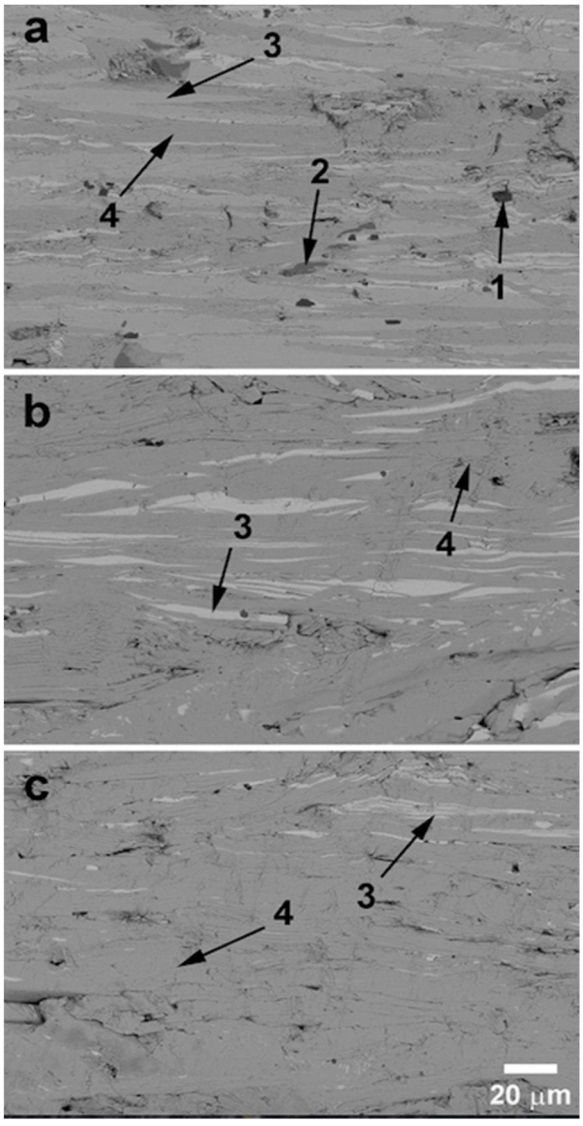

Fig. 2 – Representative FESEM micrographs of longitudinal polished surfaces of 0.10K-substituted samples (a) as-grown; and (b) annealed; and (c) 0.15K annealed ones. The numbers identify the different phases: (#1) corresponds to cobalt oxide; (#2) Bi-free phase; (#3) Co-poor phase; and (#4) thermoelectric $Bi_2Sr_2Co_2O_y$ phase.

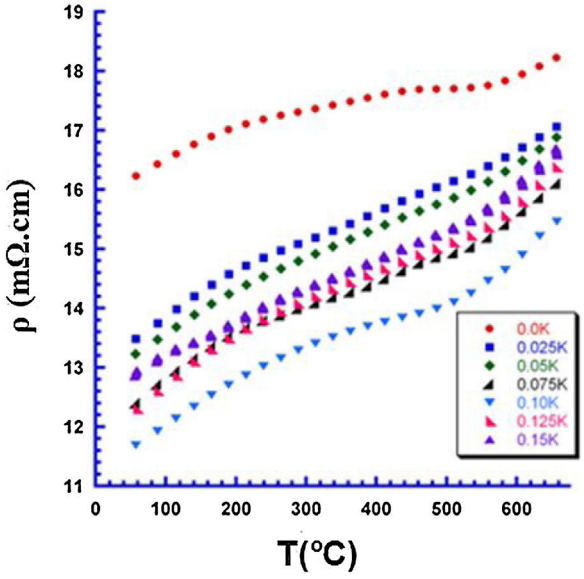

Fig. 3 – Temperature dependence of electrical resistivity for $Bi_2Sr_{2-x}K_xCo_2O_y$ annealed samples.

associated with lower radial thermal gradients when the melting point of samples is decreased. Annealed samples possess much less secondary phases, and only the Co-poor and thermoelectric phases (#3, and 4, respectively) can be identified, while the grain alignment is maintained. Furthermore, raising K-substitution produces the decrease of the amount of secondary phases. In addition, it is necessary to mention here that all samples show very few pores, which is a feature associated to the LFZ technique [47,48]. This fact has been confirmed by Archimedes method, which showed that relative samples density was around 97 ± 2%.

In Fig. 3, electrical resistivity determined on the longitudinal direction of samples after annealing, is displayed. All samples behave very similarly and show metallic characteristics ($d\rho/dT \geq 0$). This is due to the fact that texturing process promotes the formation of large amounts of oxygen vacancies [49], which can be filled during the thermal treatment. In these samples, electrical resistivity values first decrease with the K-content up to 0.10 K, slightly increasing for higher K-substitution. It is necessary to emphasize that the electrical resistivity values of K-substituted samples always are lower than in the undoped ones. It is possible to argue that this behaviour with K-doping is related with

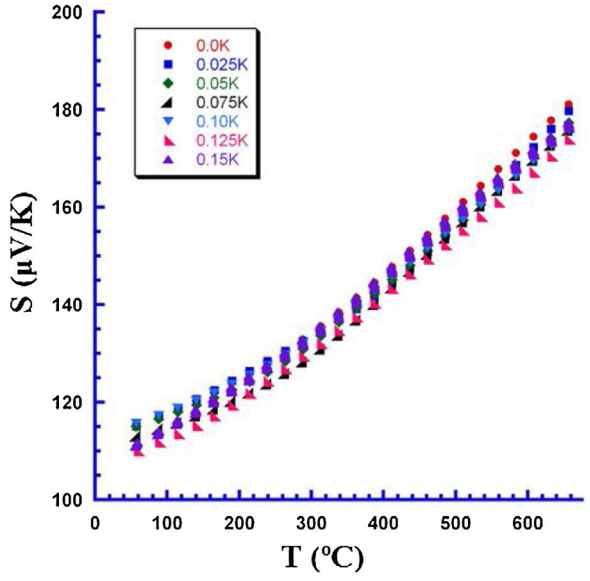

Fig. 4 – Temperature dependence of Seebeck coefficient for $Bi_2Sr_{2-x}K_xCo_2O_y$ annealed samples.

the relative importance of two contrary factors. The substitution of alkaline-earth cations by alkaline ones decreases the total charge in the RS layer, leading to the raise of Co oxidation state in the conducting one, and the hole concentration. On the other hand, their different cationic radii and weight may create defects in the crystal structure resulting in a decrease the carrier mobility. Therefore, it is considered that the first effect is the dominant one up to 0.10K-doping, while the second one is more important for further doping. At 50 °C, the minimum values were obtained in 0.10 K doped samples (11.6 mΩ cm, with around 4% uncertainty [50]). We have to emphasize at this point that this value is lower than the reported in the literature for sintered materials in different conditions (15–22 mΩ cm) [27,42], or in single crystals (18 mΩ cm) [51]. At high temperature, the lowest ρ value (14.8 mΩ cm at 650 °C, in 0.10K-substituted samples) is close to the obtained in materials sintered in oxidizing environment (~15 mΩ cm) [27]. Furthermore, it is largely lower than the reported for hot-pressed samples (~40 mΩ cm) [52].

The Seebeck coefficient variation with respect to temperature in annealed samples is displayed in Fig. 4. Taking into account the positive sign of S in the whole measured temperature range, it is clear that the conduction mechanism is mainly governed by holes. In addition, Seebeck coefficient monotonically rises with temperature with very similar values for all samples, independently of K content. At room temperature, the maximum S values were determined in 0.10K-substituted samples (115 μV/K, with about 4% uncertainty [50]). These values are consistent with the reported for materials sintered in oxidizing environment (125 μV/K) [27], single crystals (115 μV/K) [51], or hot-pressed samples (110 μV/K) [52]. On the other hand, at 650 °C, the highest value is around 180 μV/K, which is larger than the reported for hot-pressed samples (~150 μV/K) [52], and lower than the determined in sintered samples obtained by soft chemistry routes (205 μV/K) [44].

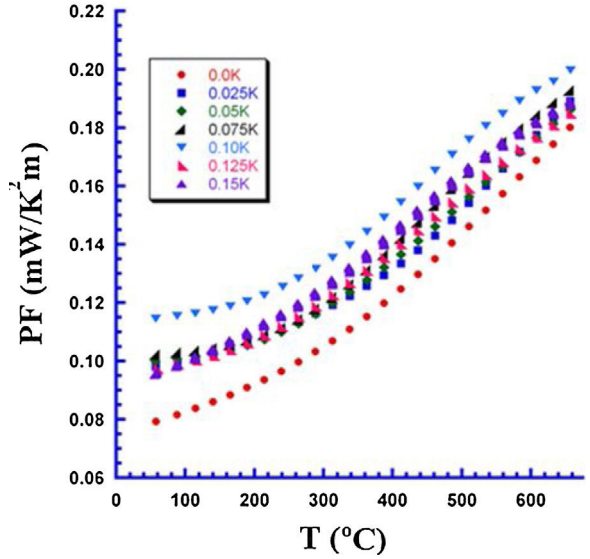

Fig. 5 – Temperature dependence of power factor for $Bi_2Sr_{2-x}K_xCo_2O_y$ annealed samples.

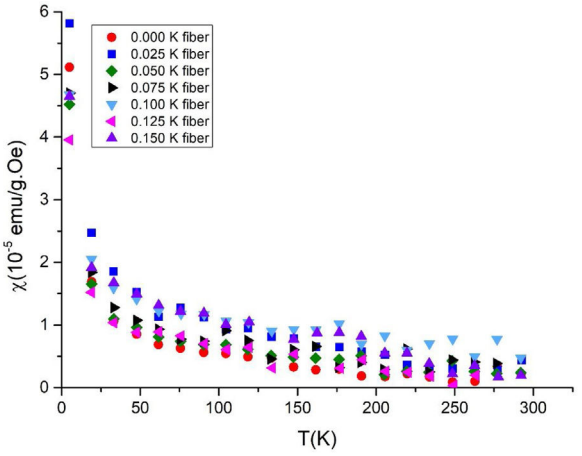

Fig. 6 – DC-magnetic susceptibility with respect to temperature for the all annealed samples measured at 20 Oe.

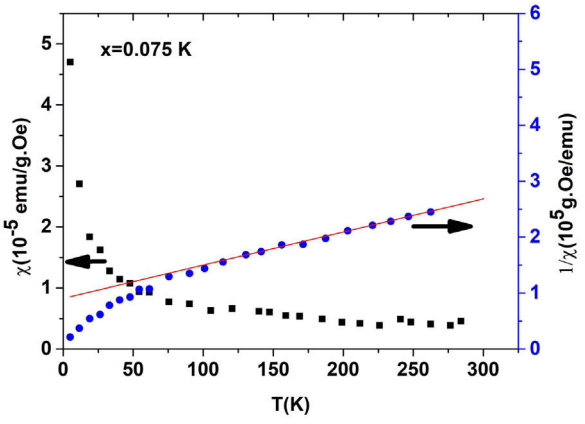

Fig. 7 – DC-magnetic susceptibility and inverse DC-magnetic susceptibility curves for the 0.075 K doped samples measured at 20 Oe.

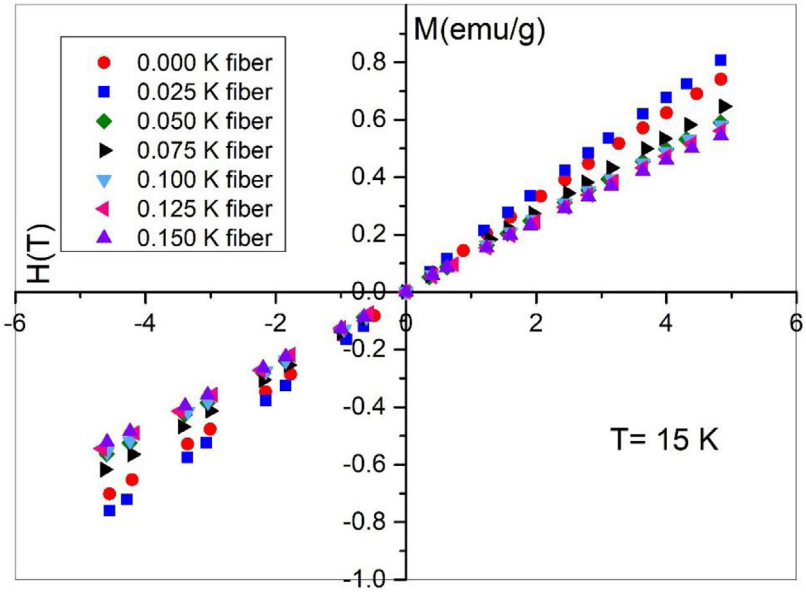

Fig. 8 – Hysteresis curves for $Bi_2Sr_{2-x}K_xCo_2O_y$ annealed samples measured at 15K.

In Fig. 5, PF variation with temperature is presented. The maximum value at room temperature (0.115 mW/K^2 m) has been achieved in 0.10K-doped samples, which is close to those measured in materials sintered in oxidizing environment (0.10 mW/K^2 m) [27], but higher than the reported for single crystals (0.07 mW/K^2 m) [49]. On the other hand, at 650 °C, the maximum PF value in 0.10K-doped samples (0.20 mW/K^2 m) is the same determined in sintered materials from precursors produced through soft chemistry routes (0.20 mW/K^2 m) [44], and is superior to the reported for hot-pressed samples (0.05 mW/K^2 m) [52].

As it is well-known, thermoelectric devices can transform heat energy into electrical one (Seebeck effect), while the reverse counterpart is known as thermoelectric cooling phenomenon (Peltier effect). On the other hand, there are some studies about the magnetic cooling effect of these materials, which is based on the Magnetocaloric Effect (MCE). This phenomenon is a new promising subject for application in refrigeration systems. Therefore, the intense scientific studies on the development of low-temperature thermoelectric refrigeration devices for optimization over wide temperature ranges has revealed as very interesting in the new thermoelectric materials [53]. In addition, thermoelectric parameters as power factor, or Seebeck coefficient, are known to be very sensitive to small fluctuations in magnetic properties. Therefore, in order to obtain new promising samples for cooling applications, the magnetic characterization of the materials is very important. In order to clearly understand the nature of magnetic phase, the magnetization versus temperature data has been recorded in zero-field cooled mode, under 20 Oe external applied magnetic field. From these experiments, very similar magnetic susceptibility (χ) values were obtained for all samples, as it can be seen in Fig. 6. In the graph, it is shown that magnetic susceptibility values for all samples sharply drop from 5 K up to 25 K, and then slowly decrease above 25 K, exhibiting a typical Curie–Weiss behaviour ($\chi = C/(T-\theta)$, where θ and C are the Curie–Weiss temperature and Curie constant, respectively).

According to this law, the high temperature data of each sample should be fitted to a straight line by plotting the inverse susceptibility ($1/\chi$) vs. T. For the sake of clarity, only the graph for the $x = 0.075$K sample is presented in Fig. 7. From the $1/\chi \rightarrow 0$ extrapolation of the high-T part of the curves, paramagnetic temperatures, θ, are negative, pointing out to antiferromagnetic fluctuations in the samples (see Table 1). However, the $\chi(T)$ curves do not explicitly exhibit a magnetic transition which can be attributed to a long-range antiferromagnetic state. In this regard, the $\chi(T)$ curves point towards the absence of long-range magnetic ordering as reported for the Bi/Ca/Co/O and Bi/Ba/Co/O cobaltites [53,54]. By using the $\mu_{eff} = [3k_BCM_w/N]^{1/2}$ equation, where, k_B, C, M_w, and N are the Boltzmann constant (1.38×10^{-16} erg/K), the Curie constants, the molecular weights of samples and the Avogadro number (6.02×10^{23} atoms/mol), respectively, the effective magnetic moments for each sample, μ_{eff}, have been calculated and tabulated in Table 1.

The magnetic hysteresis curves (M–H), determined at 15 K for all samples are shown in Fig. 8. These plots show that all samples display paramagnetic characteristics, above 15 K, as no hysteretic behaviour has been observed. In other words, the perfect linear $M(H)$ behaviour of samples clearly indicate a normal canonical paramagnetic ordering of the magnetic spins, due to the applied magnetic field at 15 K.

Conclusions

$Bi_2Sr_{2-x}K_xCo_2O_y$ ($x = 0.0$, 0.025, 0.050, 0.075, 0.100, 0.125, and 0.15) ceramics have been fabricated by a classical ceramic method, and directionally grown from the melt using a LFZ system. It has been found that the incongruent melting leads to textured materials composed by several phases, besides

the thermoelectric one. A drastic decrease of the secondary phases content has been produced by annealing the textured samples. In addition, K-doping decreases the secondary phases amount while enhancing the grains orientation. The decrease in electrical resistivity values with K-doping up to 0.10K-content reflects the microstructural modifications. On the other hand, Seebeck coefficient is practically unchanged with the K-substitution. As a consequence, the highest PF has been reached in 0.10K-substituted materials at all temperatures. These values are larger than the highest reported for materials prepared by hot-forging method. Magnetically, all samples are very similar and show a drastic fall from 5 to 25 K, followed by a smooth drop above 25 K. In addition, all dc-susceptibility curves exhibit a typical Curie–Weiss behaviour. *M–H* measurements showed that no hysteresis cycles have been produced. These data demonstrate that adequate K-doping and annealing of LFZ textured materials increase the electrical characteristics of $Bi_2Sr_2Co_2O_y$, while they do not drastically affect magnetic ones.

Acknowledgements

This work is supported by Research Fund of Çukurova University, Adana, Turkey, under grant contracts no: FDK-2016-6105 and FBI-2017-9225. M.A. Madre, M.A. Torres, and A. Sotelo acknowledge the MINECO-FEDER (MAT2017-82183-C3-1-R), and Gobierno de Aragon-FEDER (Research Group T 54-17 R) for funding. The authors wish to acknowledge the use of Servicio General de Apoyo a la Investigación-SAI, Universidad de Zaragoza.

REFERENCES

[1] G. Mahan, B. Sales, J. Sharp, Thermoelectric materials: new approaches to an old problem, Phys. Today 50 (1997) 42–47.
[2] L.E. Bell, Cooling, heating, generating power, and recovering waste heat with thermoelectric systems, Science 321 (2008) 1457–1461.
[3] M.H. Elsheikh, D.A. Shnawah, M.F.M. Sabri, S.B.M. Said, M.H. Hassan, M.B.A. Bashir, M. Mohamad, A review on thermoelectric renewable energy: principle parameters that affect their performance, Renew. Sust. Energ. Rev. 30 (2014) 337–355.
[4] C.M. Kim, Y.J. Hwang, Y.H. Ryu, US Patent US6393842, May 2002.
[5] H. Naito, Y. Kohsaka, D. Cooke, H. Arashi, Development of a solar receiver for a high-efficiency thermoionic/thermoelectric conversion system, Sol. Energy 58 (1996) 191–195.
[6] D.M. Rowe, Thermoelectrics Handbook: Macro to Nano, 1st ed., CRC Press, Boca Raton, FL, 2006.
[7] J.M. Santamaria, J. Alkorta, J.G. Sevillano, Mechanical properties of bismuth telluride (Bi_2Te_3) processed by high pressure torsion (HPT), Bol. Soc. Esp. Ceram. V 52 (2013) 137–142.
[8] H.C. Wang, J.-H. Bahk, C. Kang, J. Hwang, K. Kim, J. Kim, P. Burke, J.E. Bowers, A.C. Gossard, A. Shakouri, W. Kim, Right sizes of nano- and microstructures for high-performance and rigid bulk thermoelectrics, Proc. Natl. Acad. Sci. U.S.A. 111 (2014) 10949–10954.
[9] H.C. Wang, J. Hwang, M.L. Snedaker, I.-H. Kim, C. Kang, J. Kim, G.D. Stucky, J. Bowers, W. Kim, High thermoelectric performance of a heterogeneous PbTe nanocomposite, Chem. Mater. 27 (2015) 944–949.
[10] I. Terasaki, Y. Sasago, K. Uchinokura, Large thermoelectric power in $NaCo_2O_4$ single crystals, Phys. Rev. B 56 (1997) 12685–12687.
[11] M. Abdellahi, M. Bahmanpour, M. Bahmanpour, Modeling Seebeck coefficient of $Ca_{3-x}M_xCo_4O_9$ (M = Sr, Pr, Ga, Ca, Ba, La, Ag) thermoelectric ceramics, Ceram. Int. 41 (2015) 345–352.
[12] F. Li, J.F. Li, J.H. Li, F.Z. Yao, The effect of Cu substitution on microstructure and thermoelectric properties of $LaCoO_3$ ceramics, Phys. Chem. Chem. Phys. 14 (2012) 12213–12220.
[13] K. Rubesova, T. Hlasek, V. Jakes, S. Huber, J. Hejtmanek, D. Sedmidubsky, Effect of a powder compaction process on the thermoelectric properties of $Bi_2Sr_2Co_{1.8}O_x$ ceramics, J. Eur. Ceram. Soc. 35 (2015) 525–531.
[14] G. Constantinescu, Sh. Rasekh, M.A. Torres, M.A. Madre, J.C. Diez, A. Sotelo, Enhancement of the high-temperature thermoelectric performance of $Bi_2Ba_2Co_2O_x$ ceramics, Scr. Mater. 68 (2013) 75–78.
[15] A. Sotelo, M.A. Torres, Sh. Rasekh, M.A. Madre, J.C. Diez, Effect of precursors on the microstructure and electrical properties of $Bi_2Ba_2Co_2O_x$, J. Aust. Ceram. Soc. 53 (2017) 583–590.
[16] M.A. Bousnina, R. Dujardin, L. Perriere, F. Giovannelli, G. Guegan, F. Delorme, Synthesis, sintering, and thermoelectric properties of the solid solution $La_{1-x}Sr_xCoO_{3\pm\delta}$ ($0 \le x \le 1$), J. Adv. Ceram. 7 (2018) 160–168.
[17] H. Wang, C.L. Wang, Thermoelectric properties of Yb-doped $La_{0.1}Sr_{0.9}TiO_3$ ceramics at high temperature, Ceram. Int. 39 (2013) 941–946.
[18] Y.H. Zhu, W.B. Su, J. Liu, Y.C. Zhou, J. Li, X. Zhang, Y. Du, C.L. Wang, Effects of Dy and Yb co-doping on thermoelectric properties of $CaMnO_3$ ceramics, Ceram. Int. 41 (2015) 1535–1539.
[19] Y. Miyazaki, Crystal structure and thermoelectric properties of the misfit-layered cobalt oxides, Solid State Ionics 172 (2004) 463–467.
[20] H. Leligny, D. Grebille, O. Perez, A.C. Masset, M. Hervieu, B. Raveau, A five-dimensional structural investigation of the misfit layer compound $[Bi_{0.87}SrO_2]_2[CoO_2]_{1.82}$, Acta Crystallogr. B 56 (2000) 173–182.
[21] A. Maignan, D. Pelloquin, S. Hebert, Y. Klein, M. Hervieu, Thermoelectric power in misfit cobaltites ceramics: optimization by chemical substitutions, Bol. Soc. Esp. Ceram. V 45 (2006) 122–125.
[22] Sh. Rasekh, M.A. Torres, G. Constantinescu, M.A. Madre, J.C. Diez, A. Sotelo, Effect of Cu by Co substitution on $Ca_3Co_4O_9$ thermoelectric ceramics, J. Mater. Sci.: Mater. Electron. 24 (2013) 2309–2314.
[23] S. Butt, Y.-C. Liu, J.-L. Lan, K. Shehzad, B. Zhan, Y. Lin, C.-W. Nan, High-temperature thermoelectric properties of La and Fe co-doped Ca-Co-O misfit-layered cobaltites consolidated by spark plasma sintering, J. Alloys Compd. 588 (2014) 277–283.
[24] H.S. Hao, Q.L. He, L.M. Zhao, Thermoelectric properties of Cu-substituted $Bi_2Ca_2Co_2O_y$ misfit oxides, Adv. Mater. Res. 284-286 (2011) 2263–2267.
[25] N. Prasoetsopha, S. Pinitsoontorn, T. Kamwanna, V. Amornkitbamrung, K. Kurosaki, Y. Ohishi, H. Muta, S. Yamanaka, The effect of Cr substitution on the structure and properties of misfit-layered $Ca_3Co_{4-x}Cr_xO_{9+\delta}$ thermoelectric oxides, J. Alloys Compnd. 588 (2014) 199–205.
[26] F. Kahraman, M.A. Madre, Sh. Rasekh, C. Salvador, P. Bosque, M.A. Torres, J.C. Diez, A. Sotelo, Enhancement of mechanical and thermoelectric properties of $Ca_3Co_4O_9$ by Ag addition, J. Eur. Ceram. Soc. 35 (2015) 3835–3841.
[27] G. Çetin Karakaya, B. Özçelik, O. Nane, A. Sotelo, Sh. Rasekh, M.A. Torres, M.A. Madre, Improvement of $Bi_2Sr_2Co_2O_y$

thermoelectric performances by Na doping, J. Electroceram. 40 (2018) 11–15, http://dx.doi.org/10.1007/s10832-017-0078-x.
[28] G. Çetin Karakaya, B. Özçelik, M.A. Torres, M.A. Madre, A. Sotelo, Effects of K substitution on thermoelectric and magnetic properties of $Bi_2Sr_2Co_2O_y$ ceramic, J. Mater. Sci.: Mater. Electron. 28 (2017) 12652–12659.
[29] H. Wang, X. Sun, X. Yan, D. Huo, X. Li, J.-G. Li, X. Ding, Fabrication and thermoelectric properties of highly textured $Ca_9Co_{12}O_{28}$ ceramic, J. Alloys Compd. 582 (2014) 294–298.
[30] Sh. Rasekh, G. Constantinescu, M.A. Torres, M.A. Madre, J.C. Diez, A. Sotelo, Growth rate effect on microstructure and thermoelectric properties of melt grown $Bi_2Ba_2Co_2O_x$ textured ceramics, Adv. Appl. Ceram. 111 (2012) 490–494.
[31] Sh. Rasekh, M.A. Madre, J.C. Diez, E. Guilmeau, S. Marinel, A. Sotelo, Effect of Pb substitution on the thermoelectrical properties of textured $Bi_2Ca_2Co_{1.7}O_y$ ceramics prepared by a polymer solution method, Bol. Soc. Esp. Ceram. V 49 (2010) 371–376.
[32] L.D. Hicks, M.S. Dresselhaus, Relationship between microstructure and thermoelectric properties of $Bi_2Sr_2Co_2O_x$ bulk materials, Phys. Rev. B 47 (1993) 12727.
[33] R. Funahashi, I. Matsubara, S. Sodeoka, Thermoelectric properties of $Bi_2Sr_2Co_2O_x$ polycrystalline materials, Appl. Phys. Lett. 76 (17) (2000) 2385–2387.
[34] O. Nane, B. Ozcelik, H. Amaveda, A. Sotelo, M.A. Madre, Improvement of structural and superconducting properties of Bi-2212 textured rods by substituting sodium, Ceram. Int. 42 (2016) 8473–8477.
[35] B. Ozcelik, M. Gursul, A. Sotelo, M.A. Madre, Effect of K substitution on structural, electrical and magnetic properties of Bi-2212 system, J. Mater. Sci.: Mater. Electron. 25 (2014) 4476–4482.
[36] A. Sotelo, Sh. Rasekh, M.A. Torres, P. Bosque, M.A. Madre, J.C. Diez, Improved thermoelectric performances in textured $Bi_{1.6}Pb_{0.4}Ba_2Co_2O_y$/Ag composites, Ceram. Int. 42 (2016) 18592–18596.
[37] A. Sotelo, Sh. Rasekh, G. Constantinescu, M.A. Torres, M.A. Madre, J.C. Diez, Improvement of textured $Bi_{1.6}Pb_{0.4}Sr_2Co_{1.8}O_x$ thermoelectric performances by metallic Ag additions, Ceram. Int. 39 (2013) 1597–1602.
[38] Sh. Rasekh, F.M. Costa, N.M. Ferreira, M.A. Torres, M.A. Madre, J.C. Diez, A. Sotelo, Use of laser technology to produce high thermoelectric performances in $Bi_2Sr_2Co_{1.8}O_x$, Mater. Des. 75 (2015) 143–148.
[39] E. Combe, R. Funahashi, T. Barbier, F. Azough, R. Freer, Decreased thermal conductivity in $Bi_2Sr_2Co_2O_x$ bulk materials prepared by partial melting, J. Mater. Res. 31 (2016) 1296–1305.
[40] A. Sotelo, M.A. Torres, G. Constantinescu, Sh. Rasekh, J.C. Diez, M.A. Madre, Effect of Ag addition on the mechanical and thermoelectric performances of annealed $Bi_2Sr_2Co_{1.8}O_x$ textured ceramics, J. Eur. Ceram. Soc. 32 (2012) 3745–3751.
[41] D. Mercurio, J.C. Champarnaud-Mesjard, B. Frit, P. Conflant, J.C. Boivin, T. Vogt, Thermal evolution of the crystal-structure of the rhombohedral $Bi_{0.75}Sr_{0.25}O_{1.375}$ phase–a single-crystal neutron-diffraction study, J. Solid State Chem. 112 (1994) 1–8.
[42] D. Pelloquin, A.C. Masset, A. Maignan, C. Michel, M. Hervieu, B. Raveau, A new cobaltite with a tubular structure: $Bi_{3.7}Sr_{11.4}Co_8O_{28-d}$, the $n=2$ member of the series $(Bi_2Sr_2CoO_6)_n(Sr_8Co_6O_{16-d})$, Chem. Mater. 11 (1999) 84–89.
[43] R.J. Makkonen, Crystallographic and magnetic properties of solid solutions of $CoCo_2O_4$ and $CoCr_2O_4$, Suomen Kemistilehti A 35 (1962) 230–234.
[44] M.A. Madre, Sh. Rasekh, J.C. Diez, A. Sotelo, New solution method to produce high performance thermoelectric ceramics: a case study of Bi-Sr-Co-O, Mater. Lett. 64 (2010) 2566–2568.
[45] F.K. Lotgering, Topotactical reactions with ferrimagnetic oxides having hexagonal crystal structures, J. Inorg. Nucl. Chem. 9 (1959) 113123.
[46] F.M. Costa, N.M. Ferreira, Sh. Rasekh, A.J.S. Fernandes, M.A. Torres, M.A. Madre, J.C. Diez, A. Sotelo, Very large superconducting currents induced by growth tailoring, Cryst. Growth Des. 15 (2015) 2094–2101.
[47] N.M. Ferreira, A.V. Kovalevsky, M.C. Ferro, F.M. Costa, J.R. Frade, A new concept of ceramic consumable anode for iron pyroelectrolysis in magnesium aluminosilicate melts, Ceram. Int. 42 (2016) 11070–11076.
[48] Sh. Rasekh, A. Sotelo, M.A. Torres, P. Bosque, M.A. Madre, J.C. Diez, Thermoelectric properties of directionally grown $Bi_2Ba_2Co_2O_\delta$/Ag composites: effect of annealing, J. Mater. Sci.: Mater. Electron. 27 (2016) 12964–12973.
[49] M.A. Madre, F.M. Costa, N.M. Ferreira, S.I.R. Costa, Sh. Rasekh, M.A. Torres, J.C. Diez, V.S. Amaral, J.S. Amaral, A. Sotelo, High thermoelectric performance in $Bi_{2-x}Pb_xBa_2Co_2O_y$ promoted by directional growth and annealing, J. Eur. Ceram. Soc. 36 (2016) 67–74.
[50] A. Sotelo, F.M. Costa, N.M. Ferreira, A. Kovalevsky, M.C. Ferro, V.S. Amaral, J.S. Amaral, Sh. Rasekh, M.A. Torres, M.A. Madre, J.C. Diez, Tailoring $Ca_3Co_4O_9$ microstructure and performances using a transient liquid phase sintering additive, J. Eur. Ceram. Soc. 36 (2016) 1025–1032.
[51] T. Itoh, I. Terasaki, Thermoelectric properties of $Bi_{2.3-x}Pb_xSr_{2.6}Co_2O_y$ single crystals, Jpn. J. Appl. Phys. 39 (2000) 6658–6660.
[52] W. Shin, N. Murayama, Thermoelectric properties of (Bi, Pb)-Sr-Co-O oxide, J. Mater. Res. 15 (2000) 382–386.
[53] A. Maignan, S. Hebert, M. Hervieu, C. Michel, D. Pelloquin, D. Khomskii, Magnetoresistance and magnetothermopower properties of Bi/Ca/Co/O and Bi(Pb)/Ca/Co/O misfit layer cobaltites, J. Phys. 15 (2003) 2711–2723.
[54] M. Hervieu, A. Maignan, C. Michel, V. Hardy, N. Creon, B. Raveau, Metallicity and thermopower of the misfit cobaltite $[Bi_2Ba_{1.8}Co_{0.2}O_4]^{RS}(CoO_2)_2$, Phys. Rev. B 67 (2003) 045112.